Corrosion Science 139 (2018) 21–34

Contents lists available at ScienceDirect

Corrosion Science

journal homepage: www.elsevier.com/locate/corsci

Effect of silicate-based films on the corrosion behavior of the API 5L X80 pipeline steel

Leandro Antonio de Oliveira[a], Olandir Vercino Correa[b], Demetrio Jackson dos Santos[a], Alejandro Andrés Zúñiga Páez[a], Mara Cristina Lopes de Oliveira[a], Renato Altobelli Antunes[a,*]

[a] Universidade Federal do ABC (UFABC), Centro de Engenharia, Modelagem e Ciências Sociais Aplicadas (CECS), 09210-580, Santo André, SP, Brazil
[b] Instituto de Pesquisas Energéticas e Nucleares (IPEN), 05508-000, São Paulo, SP, Brazil

ARTICLE INFO

Keywords:
API 5L X80
Corrosion
XPS
Sodium silicate films
Pipeline steel

ABSTRACT

The aim of this work was to investigate the effect of silicate-based films on the corrosion resistance of the API 5L X80 steel in carbonate-bicarbonate solution at room temperature. The films were electrochemically obtained by anodic and cathodic treatments and by immersion in 1.0 M sodium metasilicate solution. The corrosion behavior was evaluated using electrochemical impedance spectroscopy and potentiodynamic polarization. Film morphology was examined by scanning electron microscopy. Adhesion strength was measured by pull-off tests. The chemical composition was evaluated by X-ray photoelectron spectroscopy. The anodic film yielded the best corrosion resistance (protection efficiency 83%). The protection mechanism is discussed.

1. Introduction

API 5L X80 steel is used as pipeline material for oil extraction in the recently discovered Brazilian pre-salt layer [1,2]. The presence of sulfide and chloride ions in the operation field has been shown to be a threat to these steels, since it is often related to the onset of localized corrosion processes [3–5]. Thus, these ions along with tensile stress and a susceptible metallic surface can lead to undesirable phenomena such as stress corrosion cracking (SCC), sulfide stress corrosion cracking (SSCC) and hydrogen induced cracking (HIC) [6–8]. Protective films have been considered as an alternative to reduce corrosion failures of pipeline steels in-service.

Due its availability, low cost, lack of toxicity and ability to form stable thin films, sodium silicate was extensively used as a corrosion inhibitor for steel in aqueous supply networks around 70 years ago [9–11]. The adsorption models of silicates have been reported in the literature [12,13]. The film formed in the presence of silicate ions is generally described as a two layer deposit, where the inner layer is composed mainly of iron corrosion products and the outer one is a mixture of adsorbed compounds of silica, ferrous hydroxide and silica gel [10,14–17].

The general accepted corrosion protection mechanism of silicate-based layers assumes that film formation occurs in solution as a result of adsorption on the metallic surface covered by corrosion products. The inhibition effect depends on the solution pH and silicate concentration [15,18]. Yang et al. [12] mention that negatively charged silicate anions such as $Si(OH)_3^-$ are active adsorbate species for magnetite in silicate solutions with pH above 10. Salasi et al. [15] have shown that the corrosion protection efficiency of silicate inhibitors depends on the formation of a silica layer on the metallic surface. This process, in turn, is driven by complex combination of the silica film with corrosion products and depends on the inhibitor concentration in solution. Indeed, the sorption of silicate anions on iron oxide species has been shown by several authors [12,13,18]. Jolstera et al. [13] have found that adsorption of silicate on maghemite (γ-FeOOH) surface occurs by the formation of iron-silicate surface complexes whose nature is pH-dependent. Hiemstra et al. [19] have found similar results for interaction of silicate species with goethite (α-FeOOH).

Exploring a different approach, Burstein and Souto [20] investigated the effect of anodic pretreatment of 304 stainless steel surfaces in sodium metasilicate solution on their pitting corrosion behavior. Pitting susceptibility was found to be much reduced by the anodic treatment in metasilicate solution. Authors hypothesized that such improved pitting resistance was due to the formation of some type of "capping" on the stainless steel surface upon contact with the metasilicate solution, consisting of a silica or silicate rich layer. However, the exact chemical nature of this layer was not investigated. The effectiveness of anodic treatment of different steels in metasilicate solution with regard to decreasing its surface activity and enhancing the corrosion resistance was also observed by Izquierdo et al. [21]. Nevertheless, the chemical composition of the silicate layer was not evaluated. The improved corrosion resistance of carbon steel exposed to

* Corresponding author.
E-mail address: renato.antunes@ufabc.edu.br (R.A. Antunes).

https://doi.org/10.1016/j.corsci.2018.04.035
Received 13 August 2017; Received in revised form 6 April 2018; Accepted 24 April 2018
Available online 30 April 2018
0010-938X/

silicate-based solution was also highlighted by Deodeshmukh et al. [22]. These authors studied the passivation behavior of carbon steel in 3.5 wt.% NaCl solution containing bicarbonate and silicate anions. Detailed assessment of the chemical nature of the surface films by XPS provided evidence for the formation of silica on the carbon steel surface which was related to the improved resistance to localized corrosion. Notwithstanding, the film formation route was not explored as a corrosion control parameter.

In the present work, we attempted to shed more light on this topic by producing silicate-based films through different processing routes and evaluating their effect on the corrosion behavior of API 5L X80 specimens. Up to our knowledge, there are no reports in the current literature showing the effect of silicate-based films on the corrosion behavior of pipeline steels and correlating the observed data with a detailed investigation of the chemical composition for films produced by different methods. Thus, the aim of the present work was to investigate the morphology, composition, and corrosion resistance of films obtained by different treatments on API L X80 pipeline steel specimens. The films were formed by anodic and cathodic electrochemical treatments and also by immersion in 1.0 M Na_2SiO_3 solution at room temperature. Film characterization was carried out using scanning electron microscopy (SEM) coupled to energy dispersive X-ray spectroscopy (EDS), X-ray photoelectron spectroscopy (XPS), pull-off tests, potentiodynamic polarization and electrochemical impedance spectroscopy (EIS).

2. Experimental

2.1. Material and sample preparation

The chemical composition of the API 5L X80 steel is shown in Table 1. The material was kindly supplied by Usiminas (Brazil) as a square section bar (6.25 cm^2 and length of 14 cm). The working electrodes were cut in a square section with an average area of 0.28 cm^2 and average thickness of 0.5 cm. Next, the steel piece was embedded in cold curing epoxy resin and mounted in a PVC holder. The exposed face of the electrode was abraded using silicon carbide (SiC) waterproof paper up to grit 2400, polished with 0.5 μm alumina (Al_2O_3) suspension and cleaned using deionized water, being subsequently dried in a warm air stream provided by a conventional heat gun.

2.2. Film formation

The electrolyte employed for film formation was an aqueous solution consisting of 1.0 M Na_2SiO_3 (pH 12) at room temperature. Three experiments were conducted: one immersion test and two electrochemical tests. The tests were conducted in triplicate.

A three-electrode cell set-up was used for the electrochemical tests. The counter electrode was a platinum wire and a silver/silver-chloride (Ag/AgCl) electrode as reference. The experiments were performed using an Ivium-n-Stat potentiostat/galvanostat. The working electrodes were initially reduced potentiostatically at -1.0 $V_{Ag/AgCl}$ for 5 min to remove the naturally formed oxide from the electrode surface. The films were formed using a potentiostatic technique, using two different routes: cathodic polarization at -0.8 $V_{ag/AgCl}$, -1.2 $V_{Ag/AgCl}$ and -1.6 $V_{Ag/AgCl}$ (cathodic treatments) and anodic polarization at $+0.5$ $V_{Ag/AgCl}$ + 1.0 $V_{ag/AgCl}$ and + 1.5 $V_{Ag/AgCl}$ (anodic treatments). The treatment time was 60 min for all cases. After film formation, the samples were thoroughly rinsed with deionized water and dried in the air.

Table 1
Chemical composition of API 5L X80 steel.

Mass (%)	C	Mn	Si	P	S	Nb	Al	Cr	V	Fe
	0.04	1.75	0.20	0.02	0.002	0.065	0.025	0.11	0.025	Bal.

Additionally, the samples were immersed in the 1.0 M Na_2SiO_3 solution at room temperature for 5 and 10 days to induce the spontaneous formation of the silicate-based film on the API 5L X80 pipeline steel. After being removed from the solution, the samples were thoroughly rinsed with deionized water and dried in the air.

2.2.1. Electrochemical characterization

The corrosion behavior was assessed in a solution consisting of 0.1 M $NaHCO_3$, 0.05 M Na_2CO_3 (pH 9.12). The solution was prepared with deionized water (18.2 MΩ cm) and analytical grade reagents. The testing solution was chosen due to the well-known critical role played by bicarbonate and carbonate anions in the onset of stress corrosion cracking of pipeline steels in high pH medium [23–26]. The tests were performed at room temperature. The measurements were carried out in a conventional three-electrode cell using a platinum wire as the counter-electrode and Ag/AgCl as reference using an Iviun n-Stat potentiostat/galvanostat. The open circuit potential was monitored for 30 min. Next, EIS measurements were carried out at the open circuit potential in the frequency range from 40 kHz to 10 mHz with 10 points per decade and an amplitude of the perturbation signal of ± 10 mV (rms). Following EIS, the working electrodes were subject to potentiodynamic polarization in the potential range from -300 mV (vs. OCP) to $+1.0$ $V_{Ag/AgCl}$ at a sweep rate of 1 mV s^{-1}. The tests were carried out in triplicate.

The samples were firstly evaluated using potentiodynamic polarization tests in order to identify those with the highest corrosion resistance for each one of the processing routes (films obtained by anodic, cathodic and immersion treatments). These data are presented as supplementary material (Figs. S1–S3). The values of passive current density (i_{pass}) were used as the criterion to select the conditions with the best corrosion resistance (Table S1). The best anodic film was obtained for the $+1.5$ $V_{Ag/AgCl}$ condition. For the cathodic and immersion conditions, the films obtained at -0.8 VAg/AgCl and after 10 days of immersion presented the lowest values of i_{pass}. As a consequence, the films formed at $+1.5$ $V_{Ag/AgCl}$, -0.8 VAg/AgCl and after 10 days of immersion in the 1.0 M Na_2SiO_3 at room temperature were selected for further characterization of morphology, adhesion and chemical composition. These conditions will be designated as “anodic”, “cathodic” and “immersion” films from this point up to the end of the text.

2.3. Film characterization

Cross-sectional micrographs of the silicate-coated samples were obtained by SEM (Jeol JSM-6010LA). EDS mapping analysis was carried out to reveal the distribution of Fe, Si, O and Na across film thickness.

Adhesion strength (practical adhesion) of silicate-based films to API 5L X80 steel samples was investigated by pull-off tests. Aluminum studs (15 mm-diameter) were bonded onto coated steel surfaces using thin films of epoxy adhesive, two-part Araldite 2015 (Huntsman Advanced Materials, Germany). Epoxy curing occurred at room temperature for 24 h. Then, the studs were pulled in the axial direction with respect to the coated surfaces at constant crosshead speed (1.5 mm min^{-1}) until full detachment of the epoxy films from them. Pull-off test curves (normal stress *versus* displacement) were obtained using an Instron universal testing machine, model 4465, equipped with a 1 kN load cell. Adhesion strength of the as-polished API 5L X80 surface was tested as reference.

XPS measurements were performed to investigate the surface chemistry of the API 5L X80 steel samples. XPS spectra were acquired using a Thermo Scienctific K-Alpha$^+$ spectrometer with a monochromated Al K-α X-ray source, spot diameter of 400 μm and calibrated to the adventitious C1s peak at 284.8 eV. Chemical state assessment was achieved by curve-fitting the spectra using the Avantage™ software. Depth profile experiments were also carried out by sputtering the surface of the silicate-coated steel with Ar+ ions. Each sputtering cycle

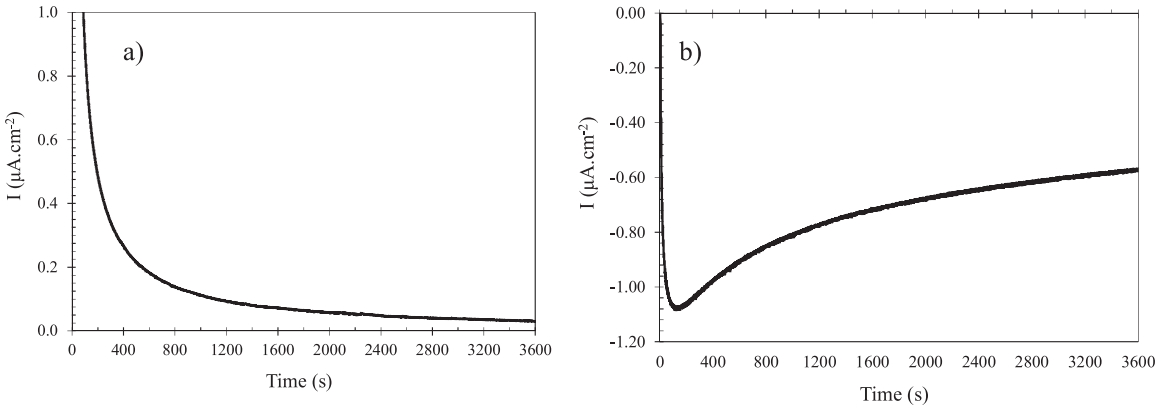

Fig. 1. Potentiostatic polarization curves of the API 5L X80 steel in 1.0 M Na_2SiO_3 solution at room temperature: a) anodic treatment; b) cathodic treatment.

consisted of 30 s Ar+ etching with energy of 3 keV. The sputter rate estimated from tantalum pentoxide (Ta_2O_5) was 0.34 nm s^{-1}. The ratio between sputter rates of Ta_2O_5 and silica (SiO_2) is 1.82 [27], giving a rough estimate of 0.19 nm s^{-1} for the films obtained in the present work.

3. Results

3.1. Film formation by the electrochemical routes

Chronoamperometric curves obtained during anodic and cathodic treatments of the API 5L X80 steel samples are shown in Fig. 1. Both treatments were conducted in 1.0 M Na_2SiO_3 solution at room temperature for 1 h. The anodic curve (Fig. 1a) shows a sharp decrease of the current density in the first 400 s, followed by a stabilization trend up to end of the test. The current densities are positive but the slope of the anodic curve is negative, indicating that the anodic reaction rate decreases on the surface of the working electrode with time. The cathodic treatment shows negative current densities during the test (Fig. 1b). The cathodic currents were gradually shifted to less negative values during film growth. Stabilization of the current density values indicates complete coverage of the steel substrate by the silicate-based films.

3.2. Open circuit potential

The corrosion behavior of the silicate-treated API 5L X80 samples was evaluated in a solution consisting of 0.1 M $NaHCO_3$ and 0.05 M Na_2CO_3 at room temperature. The open circuit potential (OCP) was initially monitored for 30 min. The results are shown in Fig. 2. The evolution of OCP with time shows a steady state condition for the as-polished API 5L X80 steel during the whole monitoring period. The film

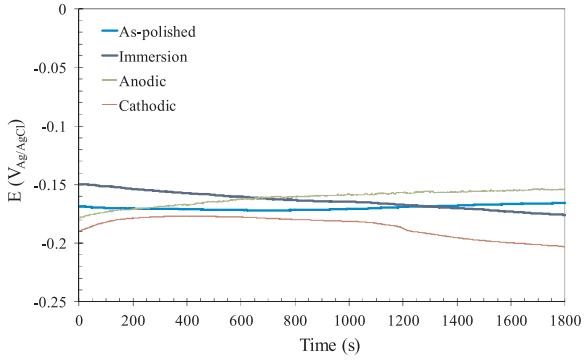

Fig. 2. Variation of the open circuit potential with time in 0.1 M $NaHCO_3$ + 0.05 M Na_2CO_3 solution at room temperature.

obtained by immersion presented a decreasing trend, indicating that surface dissolution took place over the test. The OCP is less noble than that of the as-polished steel. The film produced by cathodic deposition was the least noble, showing the most negative OCP values among the experimental conditions evaluated in the present work. The anodic treatment, in turn, yielded the noblest OCP values at the end of the test. Furthermore, there is an increasing trend of the OCP during the test, suggesting its protective nature is improved with time.

3.3. EIS measurements

Following the monitoring period of the OCP, EIS plots of the coated API 5L X80 steel were obtained in 0.1 M $NaHCO_3$ + 0.05 M Na_2CO_3 solution at room temperature. The results are shown in Fig. 3. Nyquist plots are characterized by a capacitive loop in the low frequency domain whose radius is less depressed for the anodic film. The corrosion resistance of the electrode surface is associated with the capacitive loop radius [28,29]. In this respect, the anodic treatment provided the best corrosion resistance according to the data shown in Fig. 3a. Bode plots confirmed this trend as seen in Fig. 3b. The log |Z| versus frequency plots are characterized by a negative slope of approximately -1, denoting the capacitive response of the electrochemical interface [30]. The values of log |Z| at low frequencies are related to the corrosion resistance of the electrode surface, being higher for the anodic film with respect to the other experimental conditions. The values of log |Z| for the films obtained by immersion and cathodic treatments are even lower than that of the as-polished steel. Bode phase angle plots present a highest phase angle near −80° for the as-polished, anodic and immersion films at approximately 30 Hz, indicating a deviation from the ideal capacitive response at −90° [31]. Deviation from the ideal capacitive response is even higher for the cathodic film as the maximum phase angle reaches only −75° at 1 Hz. Moreover, there is a trend of decreasing the phase angles for lower frequencies, independently of the experimental condition, suggesting the onset of charge transfer reactions in the low frequency domain. Notwithstanding, this trend is less marked for the anodic film in comparison with the other silicate-coated surfaces and the as-polished substrate. The phase angles remain more capacitive at the lowest frequencies for the anodic film, indicating a higher stability in the electrolyte and, therefore, a more corrosion resistant surface.

A more quantitative interpretation of the EIS diagrams was obtained by fitting the experimental data with an electrical equivalent circuit (EC). A two time constants model was adopted to simulate the experimental data, according to the EC shown in Fig. 4. This model provided the best fitting for all experimental conditions evaluated in the present work. For the as-polished API 5L X80 steel the physical meaning of each circuit element can be given as follows: R_1 is the electrolyte resistance; R_2 is the naturally formed oxide film resistance, Q_1 is the capacitance of

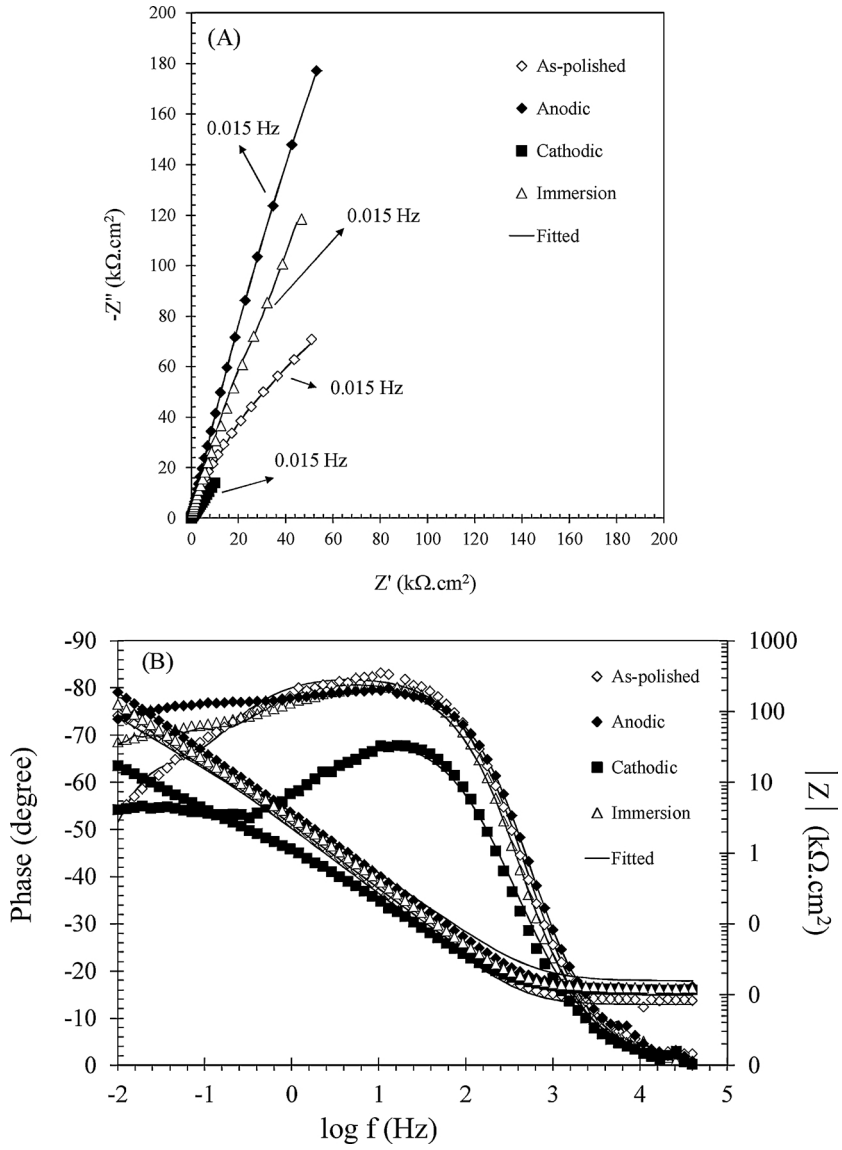

Fig. 3. EIS results of the as-polished and silicate-coated API 5L X80 steel: a) Nyquist; b) Bode plots.

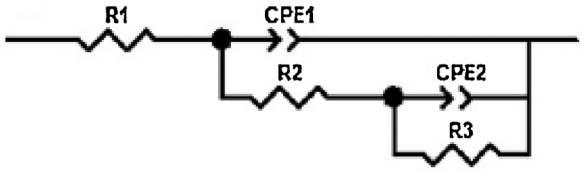

Fig. 4. Electrical equivalent circuit used to fit the experimental EIS data shown in Fig. 3.

CPE_1, modeling the capacitance associated with the oxide film. This element is related to first time constant in the medium to high frequencies. Next, a second element is used to model the charge transfer reactions at the base of the defects of the oxide film. R_3 is the charge transfer resistance, Q_2 is the capacitance of CPE_2, modeling the double layer capacitance at the interface between the metallic surface and the electrolyte. Constant phase elements (CPEs) were used instead of pure capacitors to account for surface heterogeneities [32]. The exponent of the CPE (n) is a measure of these heterogeneities, being 1 for ideal capacitors and 0.5 for diffusion-controlled processes [33]. Circuit

Table 2
Fitting parameters for the experimental EIS data of API 5L X80 steel samples in 0.1 M $NaHCO_3$ + 0.05 M Na_2CO_3 solution at room temperature.

Element	As-polished	Immersion	Anodic	Cathodic
R_1 ($\Omega\,cm^2$)	34.0 ± 15.3	33.7 ± 10.3	55.0 ± 5.2	38.7 ± 10.4
Q_1 ($10^{-5}F\,cm^2\,s^{n-1}$)	1.50 ± 0.31	2.42 ± 1.08	0.25 ± 0.10	0.52 ± 0.21
R_2 ($k\Omega\,cm^2$)	40.3 ± 13.5	13.9 ± 4.8	9524 ± 2566	7.9 ± 2.3
n_1	0.91 ± 0.03	0.91 ± 0.03	0.86 ± 0.02	0.83 ± 0.03
Q_2 ($10^{-5\ 4}F\,cm^2\,s^{n-1}$)	1.50 ± 0.35	2.40 ± 0.42	0.79 ± 0.11	0.02 ± 0.01
R_3 ($M\Omega\,cm^2$)	0.76 ± 0.17	1.30 ± 0.26	3.17 ± 0.58	0.79 ± 0.21
n_2	0.94 ± 0.02	0.92 ± 0.02	0.93 ± 0.03	0.63 ± 0.03

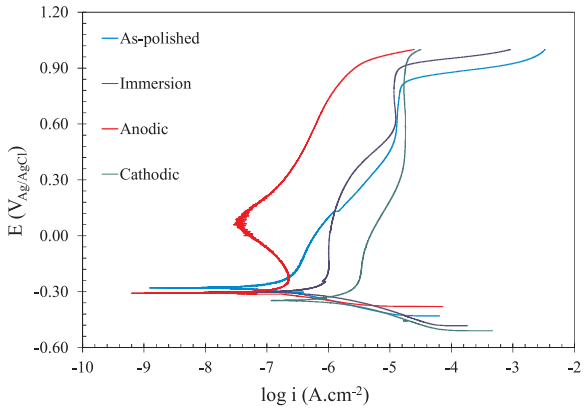

Fig. 5. Potentiodynamic polarization curves of the as-polished and silicate-coated API 5L X80 steel.

Table 3
Electrochemical parameters for the API 5L X80 steel in the as-polished and silicate-coated conditions.

Condition	E_{corr} ($mV_{Ag/AgCl}$)	i_{pass} ($\mu A\ cm^{-2}$)	η(%)
As-polished	−280 ± 12	3.09 ± 0.78	–
Immersion	−304 ± 65	2.34 ± 0.51	24 ± 3
Anodic	−308 ± 20	0.54 ± 0.02	83 ± 5
Cathodic	−347 ± 64	15.80 ± 3.56	−411 ± 15

parameters are displayed in Table 2. The impedance of a CPE is given by Eq. (1) where Q is the CPE capacitance, n is the CPE exponent, j is the complex variable and ω is the angular frequency.

$$Z_{CPE} = [Q(j\omega)^n]^{-1} \quad (1)$$

The same EC was employed to fit the experimental data of the silicate-coated samples. The circuit parameters are the electrolyte resistance, R_1, the silicate film resistance, R_2 and its capacitance Q_1, the charge transfer resistance at the film/substrate interface, R_3, accounting for the corrosion processes that take place due to electrolyte penetration through film defects and double layer pseudo-capacitance Q_2.

The sum of R_2 and R_3 is equivalent to the polarization resistance of the working electrode, being directly associated with its corrosion resistance [34]. It is clear from Table 2 that the anodic film provided the best corrosion resistance whereas the films obtained by immersion and cathodic treatments were less protective, showing even lower values of R_2 than the naturally formed oxide layer on the surface of the as-polished substrate. R_2 for the anodic film is 685 and 1202 times higher than for the immersion and cathodic films, respectively.

It is well-known that capacitance increases with the area exposed to the electrolyte [35]. Low capacitance values are associated with a more compact and corrosion resistant film. This effect can be perceived by considering the values of Q_1. The lowest value of this parameter was obtained for the anodic film. It is 52% and 90% lower than the Q_1 values of the cathodic and immersion films, respectively. The anodic treatment yielded the best coverage of the steel surface, giving rise to the lowest values of Q_1 and the highest corrosion resistance.

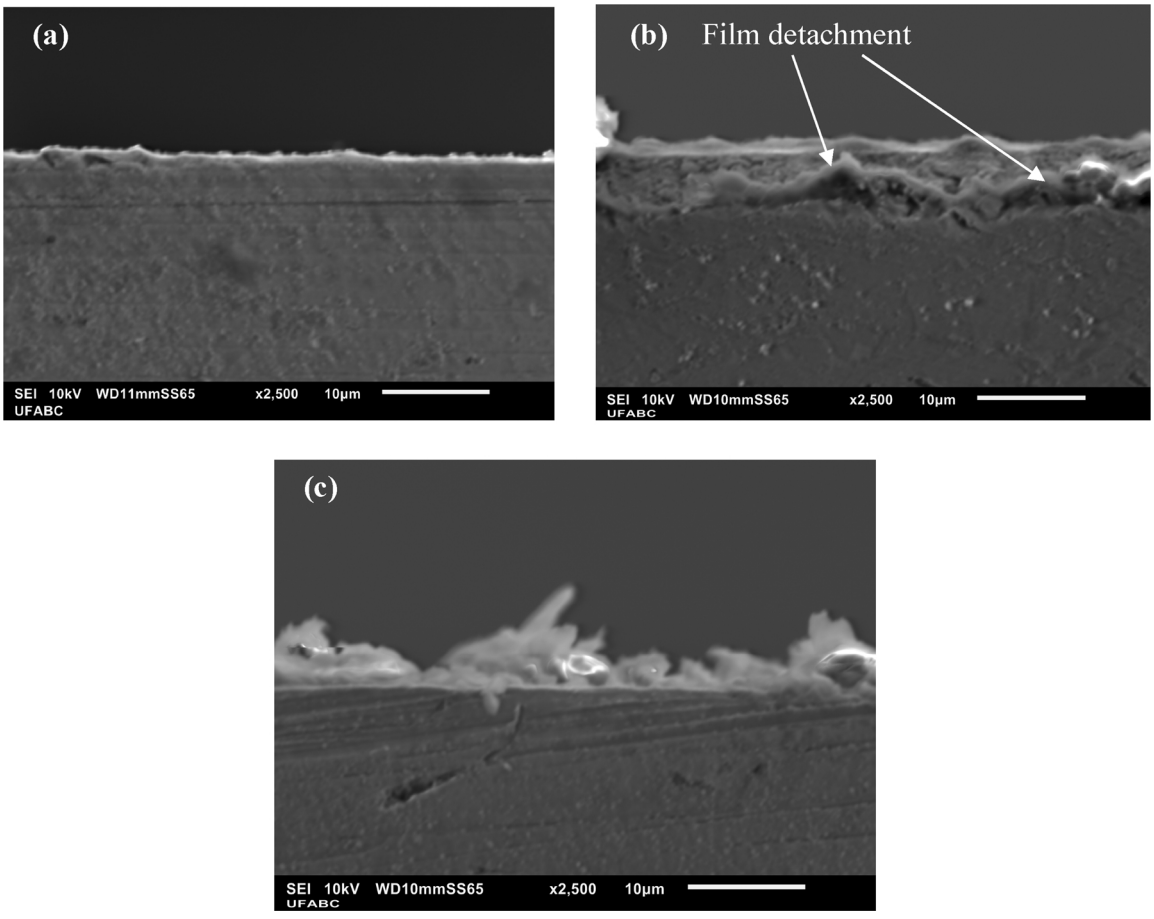

Fig. 6. SEM cross-sectional images of the silicate-coated API 5L X80 steel: a) anodic film; b) cathodic film; c) immersion film.

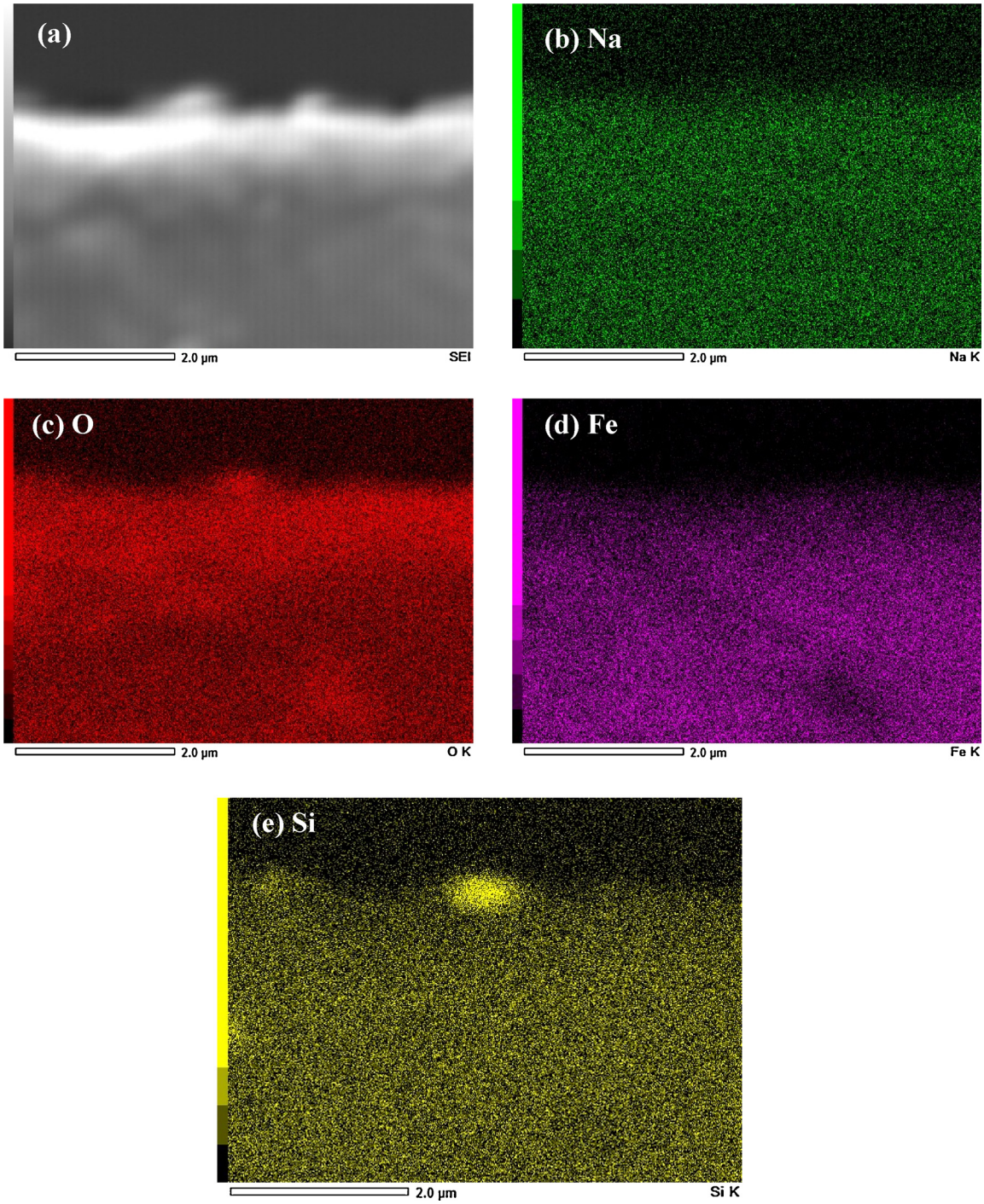

Fig. 7. (a) Cross-sectional image and EDS mapping of: (b) Na; c) O; d) Fe; e) Si for the anodic film.

3.4. Potentiodynamic polarization

Potentiodynamic polarization curves for the films obtained in sodium metasilicate solution are shown in Fig. 5. The values of corrosion potential (E_{corr}) and passive current density (i_{pass}) were determined from the curves. The results are presented in Table 3. In order to give a more quantitative interpretation of the protection efficiency (η) of each type of film, this parameter was calculated using Eq. (2), where i_{pass}° and i_{pass} are referred to the passive current density of the untreated and silicate-coated substrate, respectively.

$$\eta(\%) = \left(\frac{i_{pass}^{0} - i_{pass}}{i_{pass}^{0}}\right) x100 \quad (2)$$

The corrosion potential (E_{corr}) was slightly shifted to more cathodic values after the formation of the silicate-based films by immersion and anodic conditions. The cathodic film, in turn, presented a more intense shift toward the cathodic direction. The lower E_{corr} for the cathodic film indicates it is less stable than the films obtained by immersion or anodic treatment.

The polarization curves are typically passive independently of the surface condition as was expected due to the alkaline character of the electrolyte employed for the electrochemical tests. In this case, anodic

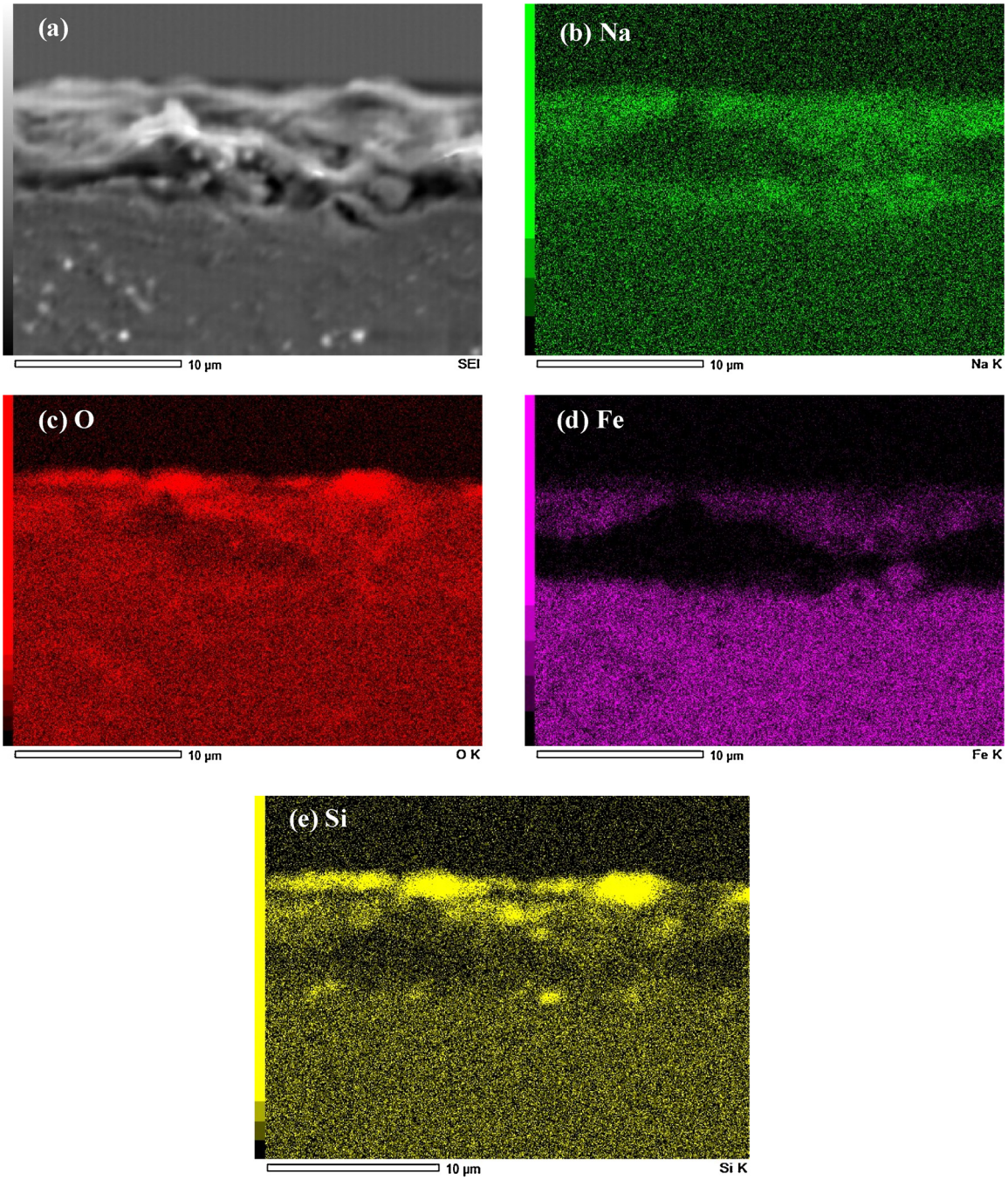

Fig. 8. (a) Cross-sectional image and EDS mapping of: (b) Na; c) O; d) Fe; e) Si for the cathodic film.

dissolution is controlled by the passive current densities [36]. These values are shown in Table 3. Following Ningshen et al. [37], i_{pass} was determined as the current density corresponding to the middle of the passive region. The lowest i_{pass} was found for the film obtained by the anodic treatment which is, therefore, the most stable condition with respect to corrosion resistance. The film formed under cathodic treatment presented the highest passive current density, indicating it is the least protective condition whereas the film obtained by immersion presented an intermediate value of i_{pass}. The protection efficiency of the anodic film is 3.45 times higher than that of the immersion film whereas the cathodic film did not protect the substrate against corrosion as indicated by its negative protective efficiency (Table 3).

Further assessment of the protection efficiency was carried out by estimating the film porosity according to the procedure described by Diaz et al. [38] and Andrade et al. [39]. Film porosity (P) can be determined based on Eq. (3) where $R_{p,s}$ is the polarization resistance of the uncoated substrate and R_p is the polarization resistance of coated material. This parameter was calculated assuming that R_p corresponds to the sum of R_2 and R_3 in Table 2. The porosity obtained for the anodic film was 6.3% while that for the immersion film was 61%. The cathodic film, in turn, did not provided a reasonable value according to Eq. (3), since it led to lower value of R_p when compared to the bare substrate, thus offering no protection against corrosion, as indicated by its negative protection efficiency (Table 3).

$$P(\%) = \left(\frac{R_{p,s}}{R_p}\right) x100 \tag{3}$$

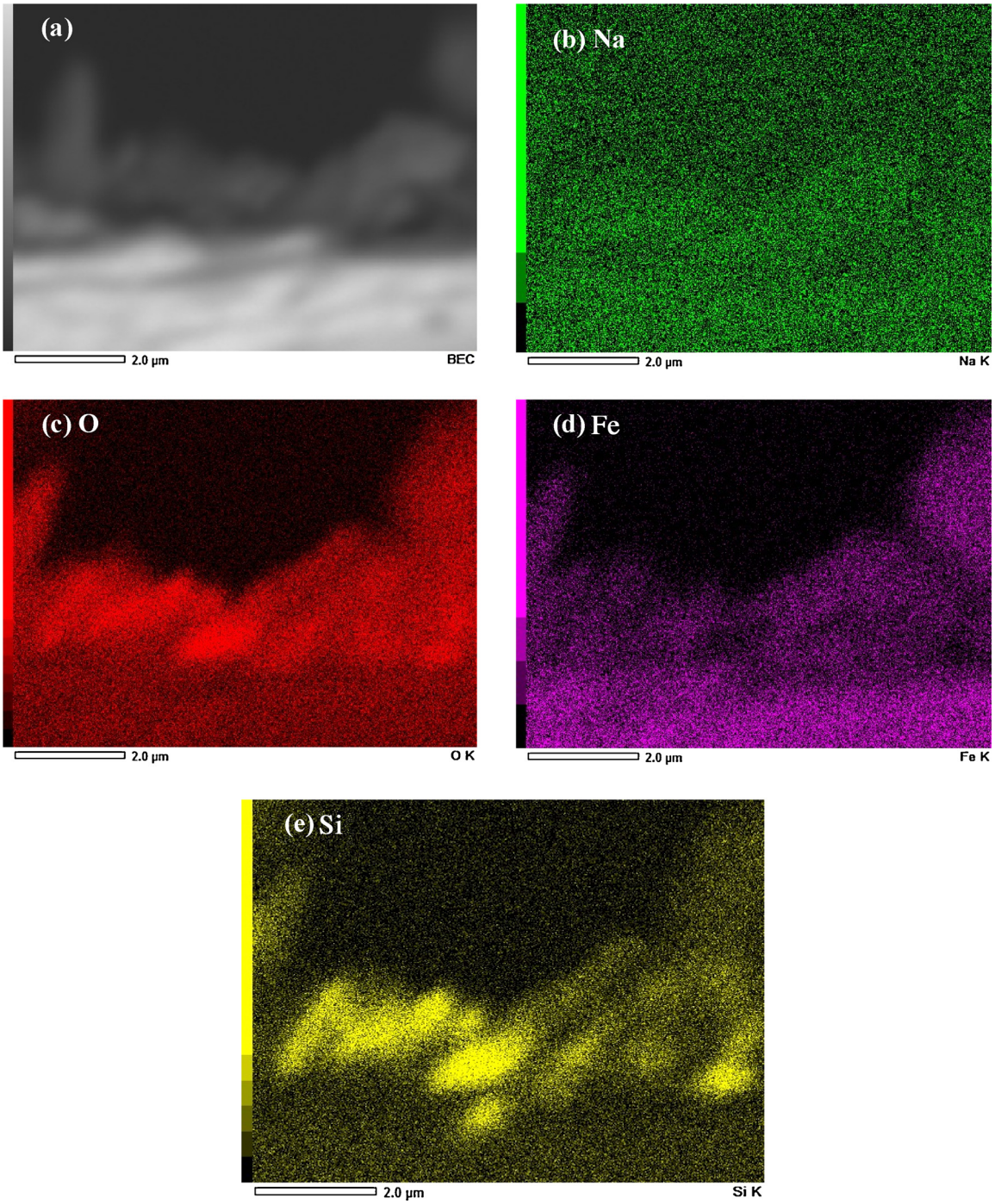

Fig. 9. (a) Cross-sectional image and EDS mapping of: (b) Na; c) O; d) Fe; e) Si for the immersion film.

3.5. SEM/EDS analysis

SEM cross-sectional images of the silicate-based films are shown in Fig. 6. The anodic film (Fig. 6a) is thin and compact. Its interface with the underlying API 5L X80 steel is continuous. The cathodic film (Fig. 6b), in turn, is not continuously distributed at the interface with the substrate. There are visible regions where it apparently detaches from the substrate, suggesting it is not well-adhered to it. The immersion film (Fig. 6c) is more evenly distributed across the interface with the substrate than the cathodic one. It is clearly, though, less compact than the anodic film.

EDS mapping obtained on the cross-section of the silicate films revealed the distribution of Si, Na and O across the film interface. EDS mapping for the anodic film (Fig. 7) shows that Si, Na and O are homogeneously distributed on the cross-section with a slightly Si enrichment near the top surface. EDS mapping for the cathodic film (Fig. 8) shows that Si and O are mainly enriched at the top surface. Differently from the anodic film, though, the distribution is not homogeneous with a clear region where the contents of all elements significantly decrease. Such region corresponds to the areas where the film is apparently detached from the metal substrate in the cross-sectional view shown in Fig. 8a. The anodic film presented a more compact morphology at the interface with the substrate. EDS mapping for the immersion film (Fig. 9) indicates that Si, O and Na are less homogeneously distributed across the interface with the substrate than the anodic layer but did not display the defective regions observed for the

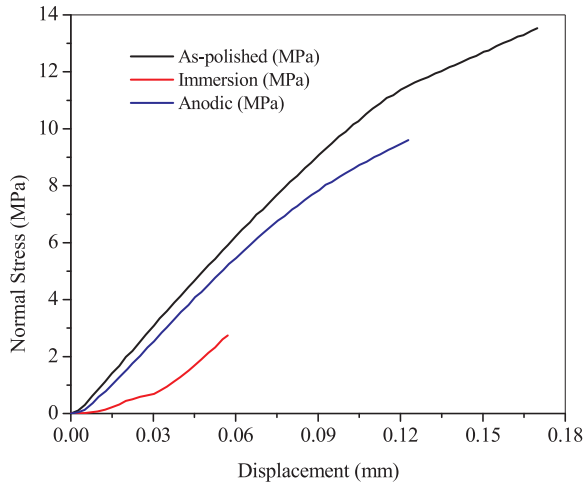

Fig. 10. Normal stress versus displacement curves for the as-polished API 5L X80 and silicate-coated samples obtained from the pull-off tests.

cathodic film.

3.6. Pull-off test

Normal stress *versus* displacement curves obtained by pull-off tests are presented in Fig. 10. The epoxy adhesive surfaces were fully covered with silicate-based films after the pull-off test. Thus, a cohesive failure of these films is believed to have occurred. The reference sample (as-polished API 5L X80 surface), in turn, revealed an adhesive failure at the epoxy/stud interface. In this case, the adhesion strength of API 5L X80/epoxy was not assessed, since the epoxy/stud interface failed earlier.

The anodic film presented the highest value of normal stress, reaching approximately 9.0 MPa. This result is in agreement with the EIS and potentiodynamic polarization measurements, since the adhesion strength to metallic substrate is strongly related to corrosion protection [40]. The adhesion strength was significantly reduced for the immersion film. Likewise, the cathodic film failed even before testing, during specimen clamping to the testing machine which precluded pull-off curve measurement for this condition. Its defective interface with the substrate (Fig. 6b) is likely to yield low adhesion strength whereas the more continuous distribution of the immersion and anodic films across the interface with the steel substrate should give rise to improved adhesion strength to the substrate.

3.7. XPS analysis

3.7.1. Core levels

High resolution XPS spectra were acquired to achieve detailed information about the surface chemistry of the different silicate-based films. The Fe2p region is shown is Fig. 11. From the patterns shown in this figure the Fe2p core levels were deconvoluted into six different components. The Fe2p core level structure is complex due to the existence of spin-orbit doublets of elemental iron, Fe^{2+}, Fe^{3+} and shake-up satellites of Fe^{2+} and Fe^{3+} species [41]. The first component at the

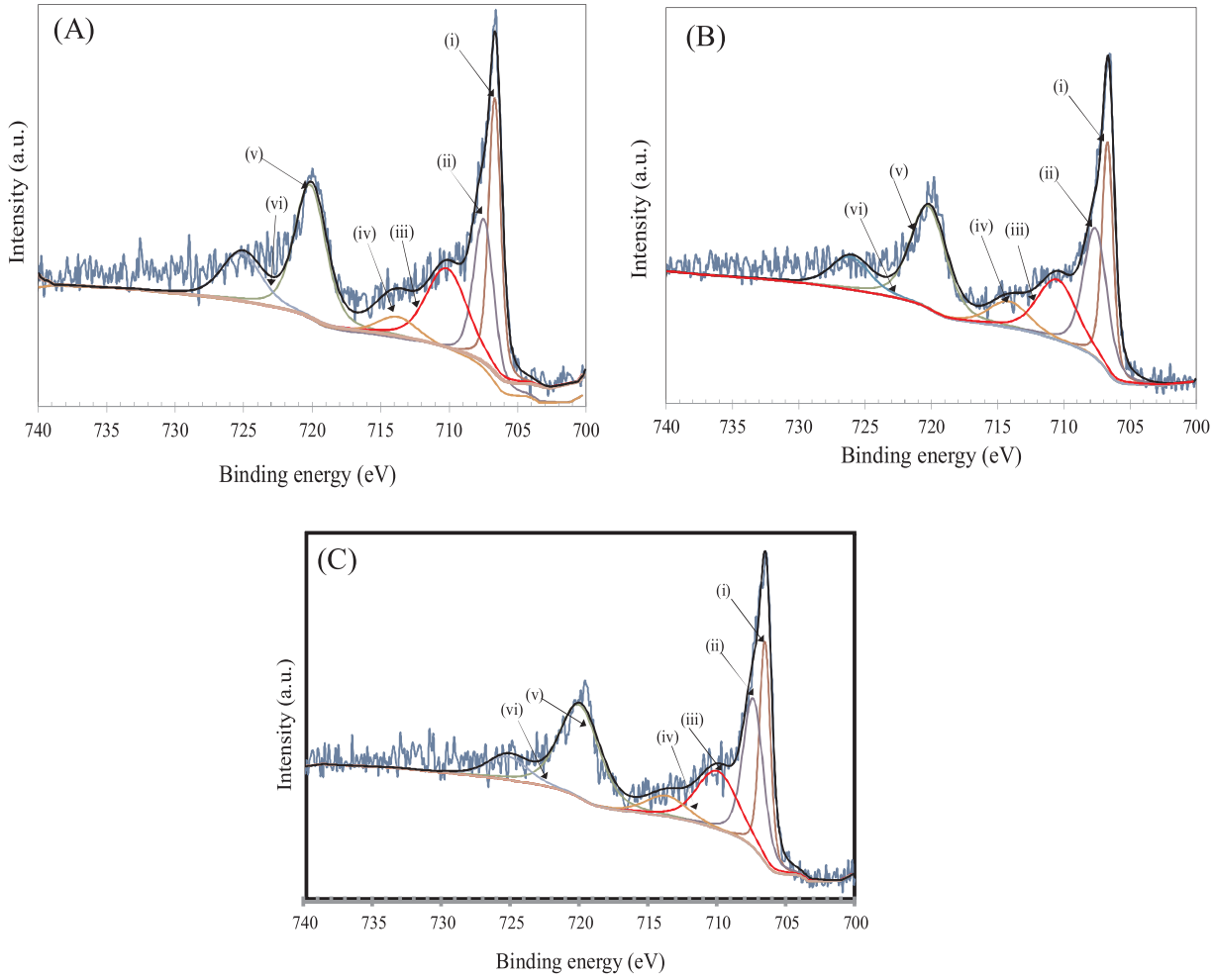

Fig. 11. XPS Fe2p core levels for the silicate-coated API 5L X80 steel: a) anodic film; b) cathodic film; c) immersion.

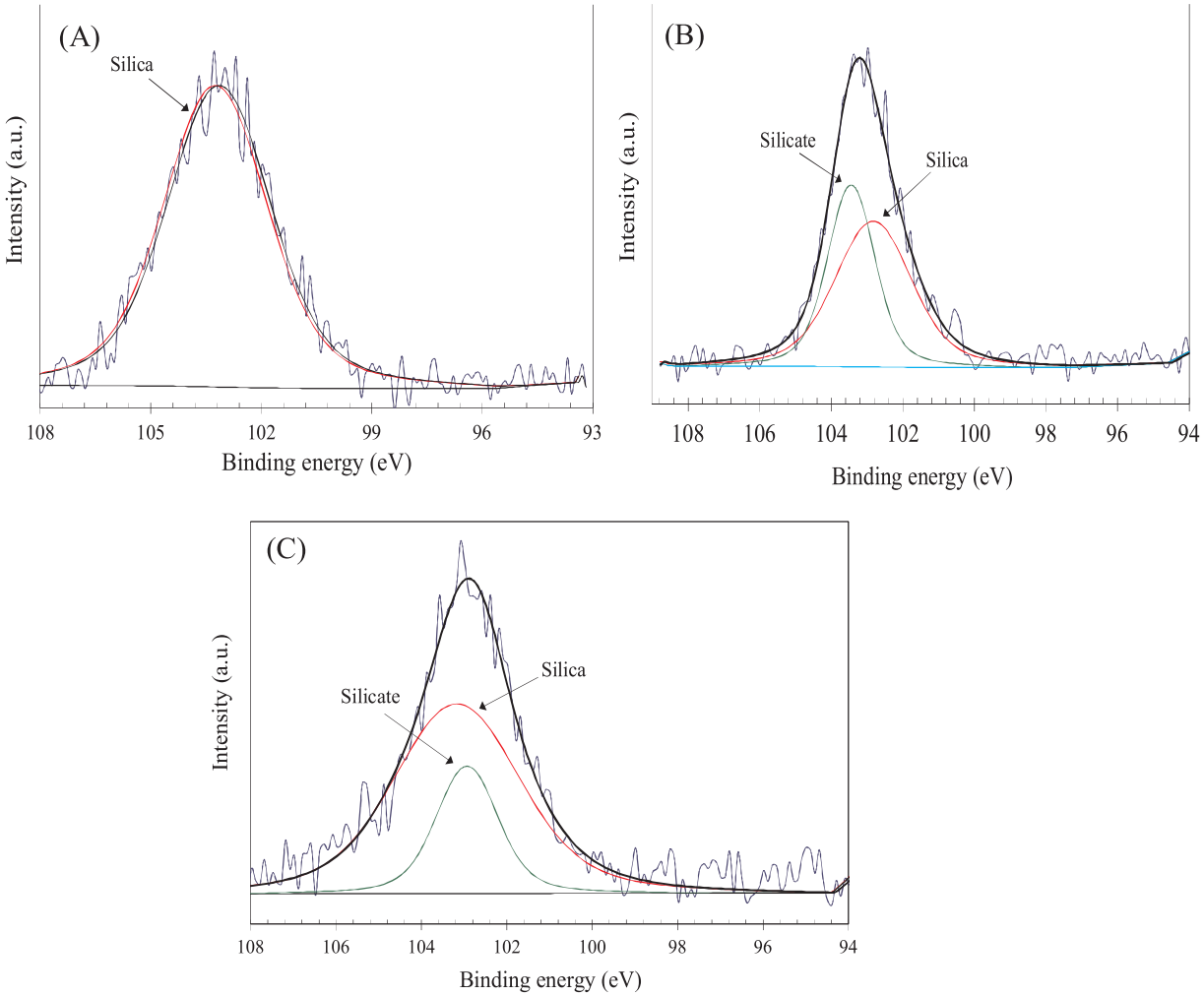

Fig. 12. XPS Si2p core levels for the silicate-coated API 5L X80 steel: a) anodic film; b) cathodic film; c) immersion.

lowest binding energy was assigned to metallic iron from the API 5L X80 steel substrate. The other signals were assigned to $Fe2p_{3/2}$ and $Fe2p_{1/2}$, corresponding to oxidized iron species. Component (ii) signal was due to a mixture of Fe^{2+} and Fe^{3+} species such as FeO, $Fe(OH)_2$, $Fe(OH)_3$, FeOOH, Fe_2O_3 and Fe_3O_4 [42,43]. Component (iii) is assigned to FeOOH species, corresponding to Fe^{3+} signal which is confirmed by the weak satellite peak (vi) assigned to $Fe2p_{1/2}$ component of Fe^{3+} [44]. Component (iv) is a broad satellite peak of $Fe2p_{1/2}$ signal, corresponding to nonstoichiometric FeOOH and Fe_2O_3 [41]. Component (v) is a pronounced satellite peak of Fe^{3+} species. The results reveal that iron is mainly present as a mixture of oxide/hydroxides, independently of the silicate-based film formation route.

The Si2p region is shown is Fig. 12. From the patterns shown in this figure the Si2p core levels were deconvoluted into two different components for the cathodic and immersion films. For the anodic film, in turn, one single component was assigned to the Si2p core level. The component with binding energy around 103 eV is assigned to silicon bonded to oxygen in the silica compound (SiO_2) where the lower binding energy component is reported for silicate-based species [45,46]. Silicon chemical state depended on the silicate treatment. Silicon was encountered exclusively as silica for the anodic film, whereas silicate and silica species were found for the cathodic and immersion-treated surfaces. The silica content was higher for the immersion-treated specimen whereas silicate species predominate for the cathodic film. The atomic concentrations are shown as supporting information in Table S2.

The Na1s core levels for the different silicate-based films are shown in Fig. 13. From the patterns shown in this figure the spectra were deconvoluted into two different components for the anodic and immersion films. For the cathodic film, in turn, one single component was assigned to the Na1s core level. The peak at 1071.4 eV for the cathodic film corresponds to Na(I) species, such as Na_2O, as reported by Yuan et al. [45]. Other authors report this component at slightly higher binding energies ranging from 1071 up to 1073 eV [47,48] which is consistent with the high binding energy component found for the anodic and immersion films. The low binding energy component of the anodic and immersion films could be related to metallic sodium. However, metallic sodium is associated with an Auger peak at approximately 492.2 eV [49,50] and the low binding energy component appears above 498 eV in the survey spectra of the silicate-based films (Fig. S4). Thus, it could not be associated with metallic sodium. It is probably related to an interface ligand between the silicate film and the steel substrate which takes place only for the anodic and immersion films.

The O1s region for the different silicate-based films is shown in Fig. 14. From the patterns shown in this figure the spectra were deconvoluted into three different components for all silicate-based films. Component (i) is assigned to O^{2-} species whereas component (ii) is due to OH- ligands. The high binding energy component is often assigned to adsorbed H_2O, OH^- or O^- species [51].

3.7.2. Depth profile experiment

XPS depth profile experiments of the silicate-coated API 5L X80 steel were performed to study the atomic concentration of the main

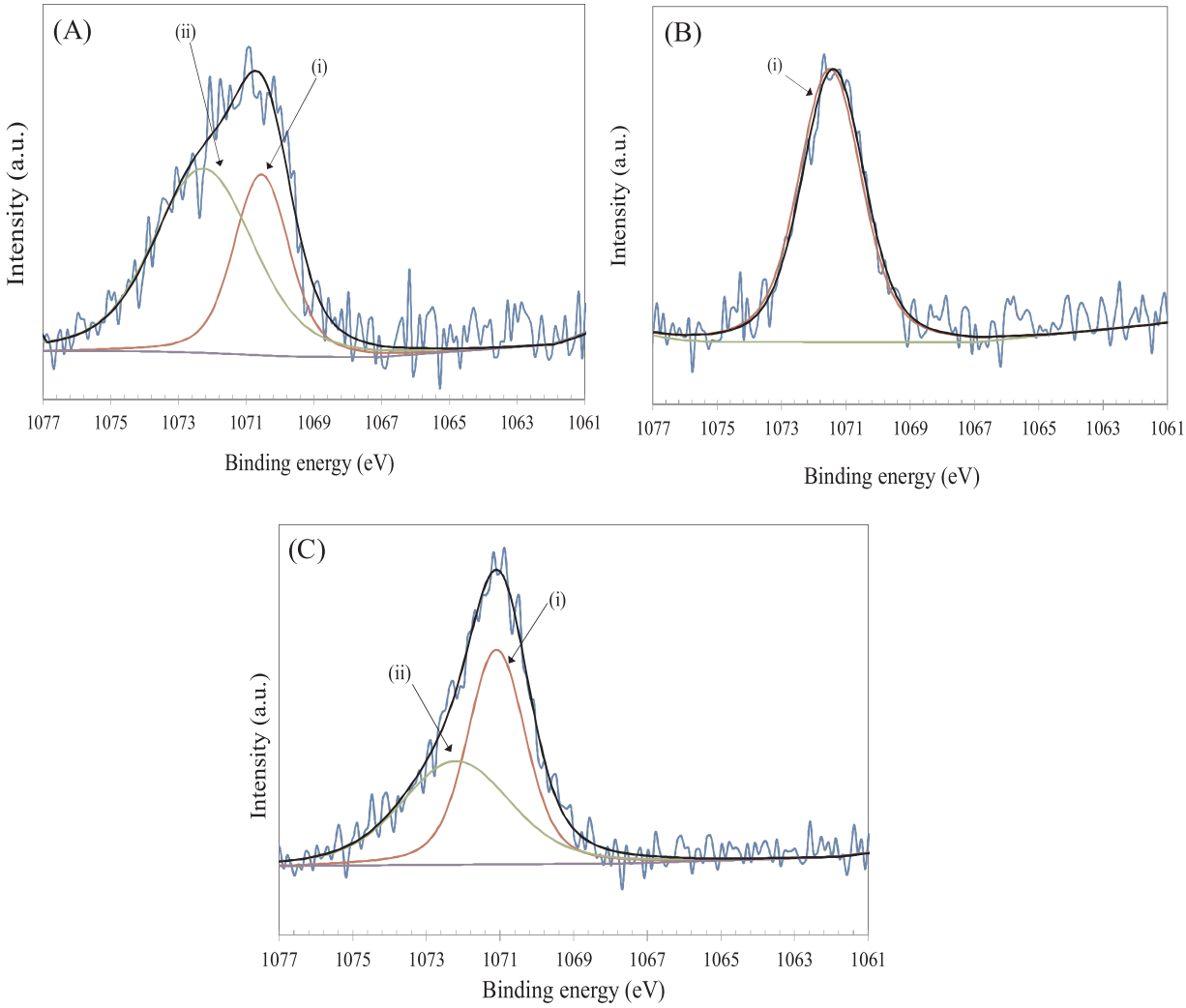

Fig. 13. XPS Na1s core levels for the silicate-coated API 5L X80 steel: a) anodic film; b) cathodic film; c) immersion.

elements in the silicate-based films as they are continuously sputtered with Ar^+ ions. Fig. 15 shows the variation of the Fe2p, Si2p, Na1s and O1s atomic concentrations with sputtering time for the anodic film. Iron atomic concentration increases with time whereas oxygen and silicon concentrations gradually decrease as the anodic film is sputtered. Sodium concentration, in turn, is rather unaffected throughout the test. The silicate-based film was not removed after sputtering as can be unequivocally perceived by the relative high silicon and sodium concentrations that are still observed at the end of the test.

Fig. 16 shows variation of the atomic concentrations of Fe2p, Si2p, Na1s and O1s with sputtering time for the cathodic film. The Fe2p signal steadily increased with the sputtering time whereas the intensity of Si2p, Na1s and O1s peaks was rapidly shortened. In fact, the atomic concentrations of Si2p and Na1s have drastically fallen after only 300 s of sputtering. At the end of the test, Fe2p concentration greatly surpassed that of the other elements, giving a clear indication that the silicate-based film formed by the cathodic treatment is more easily removed than that formed upon the anodic treatment. The low adhesion strength (Fig. 10) and defective interface with the substrate (Fig. 8) are probably related to the easy removal of the cathodic film and its low corrosion resistance. The corrosion protection ability can be, therefore, deeply affected by the type of potentiostatic polarization method employed to produce the silicate film. This will be discussed in Section 4.

Fig. 17 shows the variation of the atomic concentrations of Fe2p, Si2p, Na1s and O1s with sputtering time for the immersion film. It is noteworthy that the Fe2p signal increases, but with a much slower rate than was observed for the cathodic film. As a consequence of sputtering with argon ions the intensity of the Si2p, Na1s and O1s peaks was gradually reduced due to film removal. However, the film was not completely removed, as the Si2p and Na1s signals are still detected at the end of the experiment. In fact, the Na1s concentration was little affected by sputtering, similarly to what was observed for the anodic film. Notwithstanding, while the Si2p concentration remained higher than the Fe2p concentration during sputtering for the anodic film, the film grown by immersion presented an opposite trend. The Fe2p concentration surpassed that of the Si2p at the end of the test, but with a much lower difference than was observed for the cathodic film. These results indicate that the film grown by immersion presents an intermediate removal rate between that of the anodic and cathodic films. It is also interesting to note that silicon was more easily removed than sodium from the film surface, independently of the formation route. This suggests that silicon should be enriched in the outer part of the film and would be in direct contact with the electrolyte during corrosion. In fact, EDS mapping (Figs. 7–9) confirm this hypothesis, showing silicon enrichment at the top surfaces.

The oxygen to silicon ratio (O/Si) was determined from the XPS depth profiling results of the different silicate-based films. The results are shown in Fig. 18. It is seen that whereas the O/Si ratio is rather little affected by the sputtering process for the anodic and immersion films, it is severely affected for the cathodic film, dropping off to zero after an etch time of 300 s. Moreover, it is interesting to note that the ratio is near 2.0 for the anodic and immersion films, indicating the possible

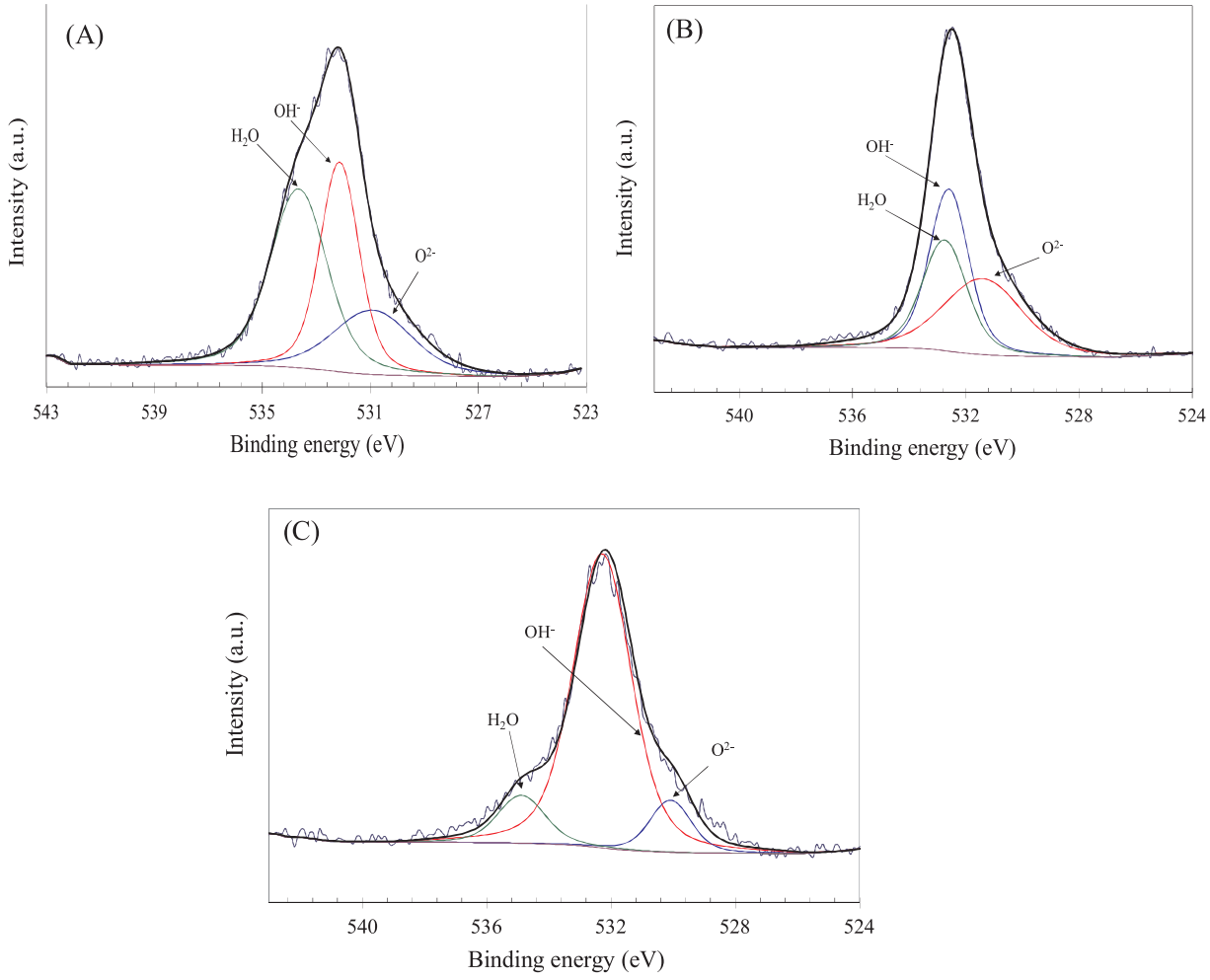

Fig. 14. XPS O1s core levels for the silicate-coated API 5L X80 steel: a) anodic film; b) cathodic film; c) immersion.

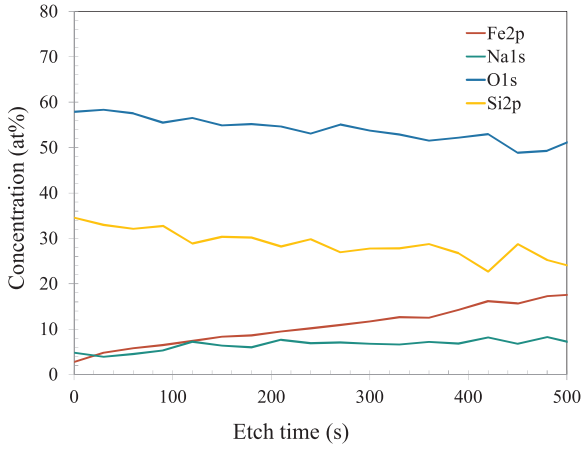

Fig. 15. Variation of the atomic concentration with the sputtering time for the main elements in the anodic film surface during depth profile experiment.

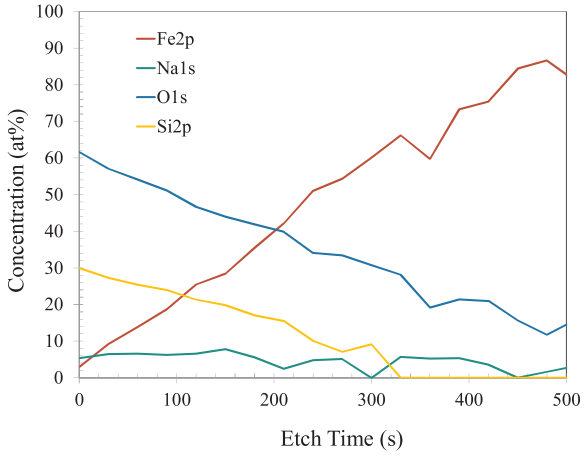

Fig. 16. Variation of the atomic concentration with the etch time for the main elements in the cathodic film surface during depth profile experiment.

presence of stoichiometric SiO_2, as indicated by the XPS high resolution Si2p spectra shown in Section 3.7.1.

4. Discussion

Electrochemical characterization of the films obtained in 1.0 M Na_2SiO_3 solution at room temperature indicated that the best corrosion resistance was obtained for the anodic treatment at +1.5 $V_{Ag/AgCl}$. The film formed by immersion for 10 days was less protective as shown in Table 3. The film obtained by the cathodic treatment at −0.8 $V_{Ag/AgCl}$ did not protect the API 5L X80 substrate against corrosion.

From the high resolution XPS spectra shown in Section 3.7.1 the Si2p region (Fig. 12) presented remarkable differences for each type of film. The anodic film showed only silica-type bonds. The immersion and cathodic films presented a mixture of silicate and silica bonds. The silica bonds prevail over the silicate bonds for the immersion film whereas an

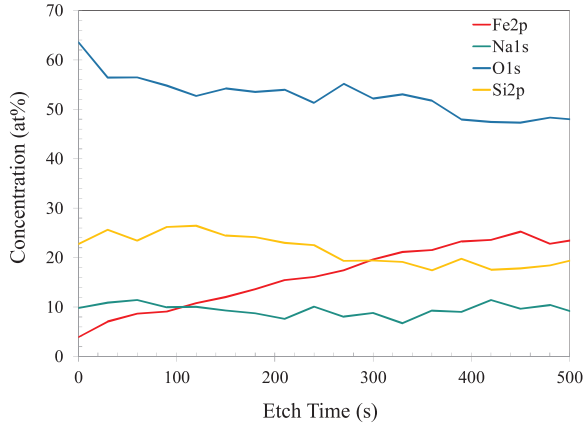

Fig. 17. Variation of the atomic concentration with the etch time for the main elements in the film grown by immersion in 1.0 M Na_2SiO_3 solution at room temperature for 10 days.

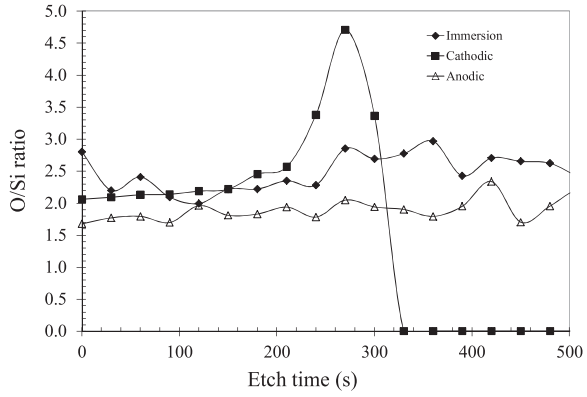

Fig. 18. O/Si ratio of the different silicate-based films as determined from the XPS depth profiling results.

opposite trend was observed for the cathodic condition. Moreover, the high resolution spectra for the Na1s region (Fig. 13) indicated the existence of a probable interface ligand between the silicate film and the steel substrate for the anodic and immersion films that was not found for the cathodic film. The presence of silica-type bonds and the interface ligand in the case of the Na1s region had a positive influence on the corrosion resistance of the coated substrate. From the depth profile experiments (Section 3.7.2) it was possible to infer that the cathodic film was much more easily removed than the films obtained by the anodic and immersion treatments. Silicon was enriched in the top layers as also confirmed by SEM/EDS analysis (Section 3.5).

At a highly alkaline pH, as that employed for the formation of the silicate-based films in the present work, anionic species are likely to be encountered in solution such as $HSiO_3^-$ and SiO_3^{2-} [52,53]. According to the literature, Fe^{2+} and Fe^{3+} ions participate in the formation of the silicate-base film on carbon steels by reacting with the silicate species in solution [54]. The presence of corrosion products on the metallic surface is considered as a determining factor for the formation of a protective silicate layer [55]. The formation of silica-rich layers is favored at high concentration of silicate anions in solution [52].

The mechanism through which the films developed in the present work are formed can be derived from the following reasoning. The presence of corrosion products on the surface of the API 5L X80 steel is not favored during the cathodic treatment, since the reducing environment does not allow extensive oxidation of the metallic surface. In this respect, as the corrosion products should react with the silicate anions on the solution to promote the formation of the silicate-based film, the cathodic treatment does not lead to a protective layer. Its relative low atomic concentration of silica-type bonds (Table S2) supports this assumption as well as its discontinuous interface with the substrate. Moreover, its relative low adhesion strength to the steel substrate (Section 3.6) and easy removal during depth profile experiments justify its poor corrosion protection ability. The film obtained by immersion, in turn, has a naturally formed corrosion product layer on its surface. Thus, during immersion, the silicate anions react with this layer, giving rise to a silicate film richer in silica (Table S2) when compared to the cathodic film. Yet, the presence of the intermediate ligand between film and substrate for the Na1s region (Fig. 13) would enhance the interaction between the silicate layer and the underlying steel surface giving rise to the slower removal rate and higher adhesion strength of the immersion film. The corrosion resistance is thereby increased with respect to the cathodic film.

The formation of corrosion products was intensified for the anodic treatment, thus promoting strong interaction with the silicate anions in solution. As a consequence, a silica-rich film was obtained as shown by the XPS results. This silica layer presented good adhesion to the substrate (Section 3.6) and was not easily removed as observed from the depth profile experiments. The formation of a silica or silicate-rich layer during anodic treatment of a ferrous alloy in 1.0 M Na_2SiO_3 was hypothesized by Burstein and Souto [20] as being responsible for the high resistance to localized corrosion observed for the samples treated in such conditions. In a similar manner, the anodic film developed in the present work owes its protective character to a silica-rich layer that is well adhered to substrate and continuously distributed across the interface with the substrate, as unequivocally shown by the results obtained by XPS, pull-off tests and SEM/EDS analysis. The oxidizing conditions of the anodic treatment were essential to sustain the formation of this layer, giving rise to a more compact and well-adhered film to the API 5L X80 substrate, thereby improving its corrosion resistance. Indeed, the compactness of the anodic and immersion films at the interface with the substrate was observed on the cross-sectional images presented in Section 3.5. The experimental data obtained by XPS, SEM/EDS and pull-off tests support the proposed mechanism for the corrosion protection ability of the films developed in this work.

5. Conclusions

Silicate-based films were formed on the surface of the API 5L X80 pipeline steel by anodic, cathodic and immersion treatments in 1.0 M NaCl solution at room temperature. The corrosion resistance of the anodic film was by far superior to that of the cathodic one, displaying a protection efficiency of 83% whereas the cathodic film did not protect the steel substrate from corrosion in 0.1 M $NaHCO_3$ + 0.05 M Na_2CO_3 solution. The immersion film presented a protection efficiency of 24%. The enhanced performance of the anodic layer against corrosion was associated with its compactness, adhesion strength and chemical composition. SEM/EDS analyses revealed the compactness and homogeneous distribution of Si, O and Na on the cross-section of the anodic film. Pull-off test indicated that the anodic layer was well-adhered to the substrate. The immersion film, in turn, presented lower adhesion strength whereas the cathodic film was poorly adhered to the substrate. The corrosion behavior was also related to the silica content on the silicate-based films, as indicated by XPS analysis. The cathodic film presented the lowest silica content. The anodic film was enriched in silica-type bonds whereas the immersion film presented a mixture of silicate and silica-type bonds but with higher silica content than the cathodic film. The mechanism through which this chemical composition affects the corrosion behavior was discussed. The interaction of the silicate anions with the steel surface was enhanced for the immersion and anodic treatments, giving rise to a silica-rich film with good adhesion and corrosion resistance. The reducing environment of the cathodic treatment did not favor the formation of a well-adhered film, thus producing a silicate-based film with poor corrosion protection ability.

Acknowledgements

The authors thank Usiminas (Brazil) for kindly providing the API 5L X80 steel sheet used in the present work and CAPES for the financial support.

Appendix A. Supplementary data

Supplementary material related to this article can be found, in the online version, at doi: https://doi.org/10.1016/j.corsci.2018.04.035.

References

[1] H.B. Xue, Y.F. Cheng, Electrochemical corrosion behavior of X80 pipeline steel in a near-neutral pH solution, Mater. Corros. 61 (2010) 756–761.
[2] H.B. Xue, Y.F. Cheng, Passivity and pitting corrosion of X80 pipeline steel in carbonate/bicarbonate solution studied by electrochemical measurements, J. Mater. Eng. Perform. 19 (2010) 1311–1317.
[3] N. Perini, P.G. Corradini, V.P. Nascimento, E.C. Passamani, M.B.J.G. Freitas, Characterization of AISI 1005 corrosion films grown under cyclic voltammetry of low sulfide ion concentrations, Corros. Sci. 74 (2013) 214–222.
[4] N. Sridhar, D.S. Dunn, A.M. Anderko, M.M. Lencka, H.U. Schutt, Effects of water and gas compositions on the internal corrosion of gas pipelines – modeling and experimental studies, Corros. Sci. 57 (2001) 221–235.
[5] A. Macias, C. Andrade, The behavior of galvanized steel in chloride-containing alkaline solutions – I. The influence of the cation, Corros. Sci. 30 (1990) 393–407.
[6] V.G. Boven, W. Chen, R. Rogge, The role of residual stress in neutral pH stress corrosion cracking of pipeline steels. Part I: pitting and cracking occurrence, Acta Mater. 55 (2007) 29–42.
[7] D.G. Li, Y.R. Feng, Z.Q. Bai, J.W. Zhu, M.S. Zheng, Influence of temperature, chloride ions and chromium element on the electronic property of passive film formed on carbon steel in bicarbonate/carbonate buffer solution, Electrochim. Acta 58 (2007) 7877–7884.
[8] E.A. Hernandez, C.M.A. Dominguez, S.R. Cabrera, M.C. Rodriguez, E.E.M. Arce, Investigations of corrosion films formed on API-X52 pipeline steel in acid sour media, Corros. Sci. 52 (2010) 2258–2267.
[9] S.T. Amaral, I.L. Muller, Effect of silicate on passive films anodically formed on iron in alkaline solution as studied by electrochemical impedance spectroscopy, Corrosion 55 (1999) 17–23.
[10] S.T. Amaral, I.L. Muller, Passivation of pure iron in alkaline solution containing silicate and sulphate – galvanostatic and potentiostatic studies, Corros. Sci. 41 (1999) 747.
[11] S.T. Amaral, I.L. Muller, A RRDE study of the electrochemical behavior of iron in solutions containing silicate and sulphate at pH 10-13, Corros. Sci. 41 (1999) 759–771.
[12] X. Yang, P. Roonasi, A. Holmgren, A study of sodium silicate in aqueous solution and sorbed by synthetic magnetite using in situ ATR-FTIR spectroscopy, J. Colloid Interface Sci. 328 (2008) 41–47.
[13] R. Jolstera, L. Gunneriusson, W. Forsling, Adsorption and surface complex modeling of silicates on maghemite in aqueous suspensions, J. Colloid Interface Sci. 342 (2010) 493–498.
[14] C.C. Davis, H.-W. Chen, M. Edwards, Modeling silica sorption to iron hydroxide, Environ. Sci. Technol. 36 (2002) 582–587.
[15] M. Salasi, T. Shahrabi, E. Roayaei, M. Aliofkhazraei, The electrochemical behavior of environment-friendly inhibitors of silicate and phosphonate in corrosion control of carbon steel in soft water media, Mater. Chem. Phys. 104 (2007) 183–190.
[16] L. Lehrman, H.L. Shuldener, The role of sodium silicate in inhibiting corrosion by film formation on water piping, J. Am. Water Works Assoc. 43 (1951) 175–188.
[17] M. Cekerevac, M. Simicic, L.N. Bujanovic, N. Popovic, The influence of silicate and sulphate anions on the anodic corrosion and the transpassivity of iron and silicon-rich steel in concentrated KOH solution, Corros. Sci. 64 (2012) 204–212.
[18] N. Jordan, N. Marmier, C. Lomenech, E. Giffaut, J.-J. Ehrhardt, Sorption of silicates on goethite, hematite and magnetite: experiments and modelling, J. Colloid Interface Sci. 312 (2007) 224–229.
[19] T. Hiemstra, M.O. Barnett, W.H. van Riemsdijk, Interaction of silicic acid with goethite, J. Colloid Interface Sci. 310 (2007) 8–17.
[20] G.T. Burstein, R.M. Souto, Improvement in pitting resistance of stainless steel surfaces by prior anodic treatment in metasilicate solution, J. Electrochem. Soc. 151 (2004) B537–B542.
[21] J. Izquierdo, B.M.F. Perez, L.M. Ruiz, V. Mena, R.R. Raposo, J.J. Santana, R.M. Souto, Evaluation of the corrosion protection of steel by anodic processing in metassilicate solution using the scanning vibrating electrode technique, Electrochim. Acta 178 (2015) 1–10.
[22] V. Deodeshmukh, A. Venugopal, D. Chandra, A. Yilmaz, J. Daemen, D.A. Jones, S. Lea, M. Engelhard, X-ray photoelectron spectroscopic analyses of corrosion products formed on rock bolt carbon steel in chloride media with bicarbonate and silicate ions, Corros. Sci. 46 (2004) 2629–2649.
[23] J.M. Sutcliffe, R.R. Fessler, W.K. Boyd, R.N. Parkins, Stress corrosion cracking of carbon steel in carbonate solutions, Corrosion 28 (1972) 313–320.
[24] B.Y. Fang, A. Atrens, J.Q. Wang, E.H. Han, Z.Y. Zhu, W. Ke, Review of stress corrosion cracking of pipeline steels in “low” and “high” pH solutions, J. Mater. Sci. 38 (2003) 127–132.
[25] A.K. Pilkev, S.B. Lambert, A. Plumtree, Stress corrosion cracking of X-60 line pipe steel in a carbonate-bicarbonate solution, Corrosion 51 (1995) 91–96.
[26] I.M. Gadala, A. Alfantazi, Electrochemical behavior of API-X100 pipeline steel in NS4, near-neutral, and mildly alkaline pH simulated soil solutions, Corros. Sci. 82 (2014) 45–57.
[27] Etch Rates of Selected Materials, Microfab, Inc., 2016 (Accessed 05 April 2018), http://www.microfabnh.com/.
[28] C. Liu, Q. Bi, H. Ziegele, A. Leyland, A. Matthews, Structure and corrosion properties of PVD CrN coatings, J. Vac. Sci. Technol. A 20 (2002) 772–780.
[29] M.F. Pillis, G.A. Geribola, G. Scheidt, E.G. de Araújo, M.C.L. de Oliveira, R.A. Antunes, Corrosion of thin, magnetron sputtered Nb_2O_5 films, Corros. Sci. 102 (2016) 317–325.
[30] M. Babaei, C. Dehghanian, M. Vanaki, Effect of additive on electrochemical corrosion properties of plasma electrolytic oxidation coatings formed on CP Ti under different processing frequency, Appl. Surf. Sci. 357 (2015) 712–720.
[31] C. Liu, Q. Bi, A. Leyland, A. Matthews, An electrochemical impedancespectroscopy study of the corrosion behaviour of PVD coated steels in 0.5NNaCl aqueous solution: part II. EIS interpretation of corrosion behaviour, Corros. Sci. 45 (2003) 1257–1273.
[32] L.J. Zhang, J.J. Fan, Z. Zhang, F.H. Cao, J.Q. Zhang, C.N. Cao, Study on the anodic film formation process of AZ91D magnesium alloy, Electrochim. Acta 52 (2007) 5325–5333.
[33] A.C. Bastos, M.G. Ferreira, A.M. Simões, Corrosion inhibition by chromate and phosphate extracts for iron substrates studied by EIS and SVET, Corros. Sci. 48 (2006) 1500–1512.
[34] R. Jindal, V.S. Raja, M.A. Gibson, M.J. Styles, T.J. Bastow, C.R. Hutchinson, Effect of annealing below the crystallization temperature on the corrosion behavior of Al-Ni-Y metallic glasses, Corros. Sci. 84 (2014) 54–65.
[35] M. Zhang, S. Mu, A. Guan, W. Li, J. Du, A high anticorrosive chromium-free conversion coating prepared with an alkaline conversion bath on electroless Ni-P coating, Appl. Surf. Sci. 349 (2015) 108–115.
[36] S. Hiromoto, E. Onodera, A. Chiba, K. Asami, T. Hanawa, Microstructure and corrosion behaviour in biological environments of the new forged low-Ni Co-Cr-Mo alloys, Biomaterials 26 (2005) 4912–4923.
[37] S. Ningshen, M. Sakairi, K. Suzuki, S. Ukai, The corrosion resistance and passive film compositions of 12%Cr and 15%Cr oxide dispersion strengthened steels in nitric acid media, Corros. Sci. 78 (2014) 322–334.
[38] B. Díaz, E. Härkonen, J. Swiatowska, V. Maurice, A. Seyeux, P. Marcus, M. Ritala, Low-temperature atomic layer deposition of Al2O3thin coatings for corrosion protection of steel: surface and electrochemical analysis, Corros. Sci. 53 (2011) 2168–2175.
[39] C. Andrade, F. Bolzoni, M. Cabeza, X.R. Nóvoa, M.C. Pérez, ElectrochemicalApproach to selected corrosion and corrosion control studies, in: L. Bonora, F. Deflorian (Eds.), European Federation of Corrosion Pub., No. 28, TheInstitute of Materials, London, 2000, pp. 332–343.
[40] S. Pourhashem, M.R. Vaezi, A. Rashidi, M.R. Bagherzadeh, Exploring corrosion protection properties of solvent based epoxy-graphene oxide nanocomposite coatings on mild steel, Corros. Sci. 115 (2017) 78–92.
[41] Th. Mayer, Black spots on carbon steel after contact to lubricating oil with extreme pressure additives: an XPS study, Appl. Surf. Sci. 179 (2001) 257–262.
[42] P. Galicia, N. Batina, I. González, The relationship between the surface composition and electrical properties of corrosion films formed on carbon steel in alkaline sour medium: an XPS and EIS study, J. Phys. Chem. B 110 (2006) 14398–14405.
[43] J.K. Heuer, J.F. Stubbins, An XPS characterization of $FeCO_3$ films from CO_2 corosion, Corros. Sci. 41 (1999) 1231–1243.
[44] A. Abidov, B. Allabergenov, J. Lee, H.-W. Jeon, S.-W. Jeong, S. Kim, X-ray photoelectron spectroscopy characterization of Fe doped TiO_2 photocatalyst, Int. J. Mater. Mech. Manuf. 1 (2013) 294–296.
[45] M.-R. Yuan, J.-T. Lu, G. Kong, Effect of SiO_2:N_2O molar ratio of sodium silicate on the corrosion resistance of silicate conversion coatings, Surf. Coat. Technol. 204 (2010) 1229–1235.
[46] M.D. Yuniati, T. Hirajima, H. Miki, K. Sasaki, Silicate covering layer on pyrite surface in the presence of silicon-catechol complex for acid mine drainage prevention, Mater. Trans. 56 (2015) 1733–1741.
[47] J.P. Lukaszewicz, X-ray photoelectron spectroscopy studies of sodium modified carbon films suitable for use in humidity sensors, J. Mater. Sci. 32 (1997) 6063–6068.
[48] R. Würz, M. Rusu, Th. Schedel-Niedrig, M.C. Lux-Steiner, H. Bluhm, M. Hävecker, E. Kleimenov, A. Knop-Gericke, R. Schlögl, In-situ X-ray photoelectron spectroscopy study of the oxidation of CuGaSe2, Surf. Sci. 580 (2005) 80–94.
[49] C. Zhu, Z. Osherov, M.J. Panzer, Surface chemistry of electrodeposited Cu_2O films studied by XPS, Electrochim. Acta 111 (2013) 771–778.
[50] D.W. Niles, K. Ramanathan, F. Hasoon, R. Noufi, B.J. Tielsch, Na impurity chemistry in photovoltaic CIGS thin films: investigation with X-ray photoelectron spectroscopy, J. Vac. Sci. Technol. A 15 (1997) 3044–3049.
[51] N. Ochoa, G. Baril, F. Moran, N. Pébère, Study of the properties of a multi-component inhibitor used for water treatment in cooling circuits, J. Appl. Electrochem. 32 (2002) 497–504.
[52] S.P. Kamaraguru, B. Veeraraghavan, B.N. Popov, Development of an electroless method to deposit corrosion-resistant silicate layers on metallic substrates, J. Electrochem. Sci. 153 (2006) B253–B259.
[53] J.-R. Chen, H.-Y. Chao, Studies on carbon steel corrosion in molybdate and silicate solutions as corrosion inhibitors, Surf. Sci. 247 (1991) 352–359.
[54] O. Lopez-Garrity, G.S. Frankel, Corrosion inhibition on AA2024-T3 by sodium silicate, Electrochim. Acta 130 (2014) 9–21.
[55] S. Giordana, I. Mabille, C. Fiaud, Inhibiting effect of silicates on corrosion of low silicon alloyed steels in neutral non-oxidising conditions at 90°C, Corros. Eng. Sci. Technol. 38 (2003) 291–297.